# Viscoelastic model for the dynamic structure factors of binary systems

N. Anento
*Departament de Física Fonamental, Universitat de Barcelona, 08028 Barcelona, Spain*

L. E. González and D. J. González
*Departmento de Física Teórica, Universidad de Valladolid, 47011 Valladolid, Spain*

Y. Chushak
*Department of Chemistry, University of Michigan, Ann Arbor, Michigan 48109, USA*

A. Baumketner*
*Department of Chemistry and Biochemistry, University of California, Santa Barbara, California 93106, USA*
(Received 27 April 2004; published 14 October 2004)

This paper presents the viscoelastic model for the Ashcroft-Langreth dynamic structure factors of liquid binary mixtures. We also provide expressions for the Bhatia-Thornton dynamic structure factors and, within these expressions, show how the model reproduces both the dynamic and the self–dynamic structure factors corresponding to a one-component system in the appropriate limits (pseudobinary system or zero concentration of one component). In particular we analyze the behavior of the concentration-concentration dynamic structure factor and longitudinal current, and their corresponding counterparts in the one-component limit, namely, the self–dynamic structure factor and self–longitudinal current. The results for several lithium alloys with different ordering tendencies are compared with computer simulation data, leading to a good qualitative agreement, and showing the natural appearance in the model of the fast sound phenomenon.

DOI: 10.1103/PhysRevE.70.041201 PACS number(s): 61.20.Lc, 61.20.Gy, 61.20.Ja, 61.25.Mv

## I. INTRODUCTION

The development of inelastic neutron scattering (INS) techniques opened up, around 40 years ago, the experimental study of the dynamic properties of several condensed matter systems, in particular of liquids. In principle the total scattered intensity in an INS experiment includes both incoherent and coherent contributions, which are related, respectively, to the self–dynamic structure factors and the dynamic structure factors. A clearcut separation of both contributions is not always possible and in the analysis of the raw data it is useful to have simple models for the dynamic and/or self–dynamic structure factors in order to achieve such a separation through a numerical fitting procedure, and perform a proper interpretation of the experimental data. Even in those cases where there is coherent scattering only, it may happen that the particular behavior of the dynamic structure factor as a function of frequency obscures the analysis, for instance when no clear side peaks appear; in this case again the availability of models for fitting helps in the interpretation of the mechanisms controlling the behavior of the dynamic properties of the system. Similar problems are encountered when the dynamic properties of liquid systems are studied by either inelastic x-ray scattering (IXS) or molecular dynamics (MD) simulations. Even though IXS produces coherent scattering only, and MD provides very detailed information of the properties of interest, nevertheless the interpretation of the numerical data obtained is greatly aided if theoretical models are available.

In this respect, and for pure systems (one-component systems), a prominent role has been played by the so called viscoelastic model, introduced by Lovesey, which basically describes the dynamic structure factor as a sum of three Lorentzian functions of frequency, one of them representing particle diffusion and the other two describing damped propagation of collective excitations. This model applies for intermediate wave vectors $k$ between those corresponding to a hydrodynamic behavior (low $k$ where the hydrodynamic model is applicable) and those corresponding to an ideal gas behavior (large $k$, where the free-particle model is correct). A similar expression is also available for the self–dynamic structure factor, but its use has been much more scarce in the literature, although as we shall show below, the viscoelastic model for the self–dynamic structure factor in fact has very interesting properties that other models lack.

The case of mixtures is more complicated. Although both the hydrodynamic and the free-particle models are readily extended to mixtures, there is no well-behaved model so far to describe the intermediate $k$ range. A previous attempt to extend the viscoelastic model to liquid mixtures [1] failed because some errors in the derivation made it incorrect, and therefore inapplicable. In particular the model did not recover the one-component case for pseudobinary systems, i.e., those systems which are in fact one component, but with some particles labeled differently from others (some of them are named type 1 and the rest type 2).

In this paper we extend the viscoelastic model to mixtures, and in particular to binary mixtures, in a consistent way which reduces to the correct one-component limit in the

*Permanent address: Institute for Condensed Matter Physics, 1 Svientsitsky Str., Lviv 79011, Ukraine.

 

appropriate cases (pseudobinary mixture or zero concentration of one component). Moreover, we give expressions for the so called Bhatia-Thornton dynamic structure factors, which are very useful when discussing ordering properties of binary systems. From these expressions it is easy to show the reduction to the one-component case, leading not only to the dynamic structure factor, but also to the self–dynamic structure factor of pure systems.

We compare the results of the model with MD data for three different types of systems: the first is a pseudobinary alloy, namely, pure liquid Li, the second corresponds to Li -Mg, which is a typical quasi-ideal system, and finally the third one corresponds to $Li_4Pb$, which is an archetypical case for a class of compound forming alloys. The case of systems with tendency to phase separation has already been considered before [2], in the study of liquid $Li_{0.61}Na_{0.39}$, which is again a typical phase separating mixture. Although apparently trivial, the study of the pseudobinary case leads to interesting conclusions regarding the behavior of the self–dynamic structure factor, which vindicate the use of the viscoelastic model for the self–dynamic structure factor of one-component systems.

## II. FORMALISM

### A. One-component system

Here we merely recall the expressions for the dynamic properties we are interested in for one-component systems. The basic magnitude to be considered is the intermediate scattering function (ISF), $F(k,t)$, which describes the collective dynamic behavior of the system and is defined as $F(k,t)=\langle \rho_{\vec{k}}(t)\rho_{-\vec{k}}(0)\rangle$, where $\rho_{\vec{k}}(t)$ is the microscopic number density,

$$\rho_{\vec{k}}(t) = \frac{1}{\sqrt{N}}\sum_{\ell=1}^{N} \exp[i\vec{k}\cdot\vec{r}_\ell(t)]$$

of the system composed of $N$ particles at positions $\vec{r}_\ell(t)$, which are enclosed in a volume $V$, so that the ionic number density is $\rho=N/V$. The initial value of the ISF is the static structure factor $S(k)$, which is directly related to the pair distribution function $g(r)$:

$$F(k,0) = S(k) = 1 + \rho \int d\vec{r}\,[g(r) - 1]\exp[-i\vec{k}\cdot\vec{r}]. \quad (1)$$

A similar separation into two terms is also possible for all times,

$$F(k,t) = F_s(k,t) + F_d(k,t), \quad (2)$$

where we have introduced the self–intermediate scattering function (SISF) $F_s(k,t)$, and the distinct intermediate scattering function $F_d(k,t)$, which obviously have the initial values $F_s(k,0)=1, F_d(k,0)=S(k)-1$. The SISF is of interest by itself, since it is the basic magnitude that describes the one-particle dynamic behavior of the system.

The dynamic structure factor (DSF) $S(k,\omega)$ and the self–dynamic structure factor (SDSF) $S_s(k,\omega)$ are obtained from the corresponding intermediate scattering functions by passing to the Fourier domain:

$$S(\vec{k},\omega) = \frac{1}{2\pi}\int_{-\infty}^{\infty} dt\; e^{i\omega t}\, F(\vec{k},t) = \frac{1}{\pi}\mathrm{Re}\tilde{F}(\vec{k},z=-i\omega) \quad (3)$$

where Re stands for the real part and $\tilde{F}(\vec{k},z)$ is the Laplace transform of $F(\vec{k},t)$, i.e.,

$$\tilde{F}(\vec{k},z) = \int_0^{\infty} dt\; e^{-zt}\, F(\vec{k},t). \quad (4)$$

The memory functions of the ISF, $M(k,t)$, and of the SIFS, $M_s(k,t)$, are then introduced through the generalized Langevin equations, which read in the time domain and in the Laplace domain

$$\frac{d}{dt}F(\vec{k},t) = -\int_0^t d\tau\, M(\vec{k},\tau)F(\vec{k},t-\tau), \quad (5)$$

$$\tilde{F}(\vec{k},z) = [z + \tilde{M}(\vec{k},z)]^{-1}F(\vec{k},t=0), \quad (6)$$

with equivalent equations for the self-counterparts. The higher order memory functions are introduced exactly in the same way: the second order memory functions $N(k,t)$ and $N_s(k,t)$ are the memory functions of $M(k,t)$ and $M_s(k,t)$, respectively, while the third order memory functions, $K(k,t)$ and $K_s(k,t)$, are the memory functions of $N(k,t)$ and $N_s(k,t)$, respectively. The initial values of the memory functions which appear in the Laplace formulation of the generalized Langevin equation are easily determined in terms of the $n$th frequency moments of the DSF and SDFS, $\omega^n(\vec{k}) = \int_{-\infty}^{\infty} \omega^n S(\vec{k},\omega)d\omega$,

$$M(\vec{k},t=0) = \omega^2(\vec{k})\omega^0(\vec{k})^{-1}, \quad (7)$$

$$N(\vec{k},t=0) = \omega^4(\vec{k})\omega^2(\vec{k})^{-1} - \omega^2(\vec{k})\omega^0(\vec{k})^{-1}, \quad (8)$$

with again equivalent expressions for the self-counterparts. Moreover, these frequency moments up to the fourth can be determined from the knowledge of only the temperature $T$, the atomic mass, the interatomic pair potential $\phi(r)$, and the static structure, i.e., $g(r)$ and $S(k)$.

A useful feature of a memory function is that it decays in time more rapidly than the function from which it originates. Based on this, it seems plausible that at some level of the hierarchy of memory functions an approximation where the memory function is just a Dirac $\delta$ function at $t=0$ should be a good ansatz. In the viscoelastic model the level at which this ansatz is taken is the third, i.e., it is assumed that

$$K(\vec{k},t) = K(\vec{k})\delta(t) \Rightarrow \tilde{K}(\vec{k},z) = K(\vec{k}),$$

$$K_s(\vec{k},t) = K_s(\vec{k})\delta(t) \Rightarrow \tilde{K}_s(\vec{k},z) = K_s(\vec{k}). \quad (9)$$

Explicit expressions of $K(\vec{k})$ and $K_s(\vec{k})$ in terms of the same magnitudes as the frequency moments can be obtained [3,4] by imposing that in the free-particle limit ($k\to\infty$) the

theory recovers the known exact $S(k,\omega=0)=S_s(k,\omega=0)$. Further details are given in the next section.

Introducing in Eq. (6) the higher order memory functions up to the third it is found that

$$\tilde{F}(\vec{k},z)=\frac{F(\vec{k},t=0)}{z+\dfrac{M(\vec{k},t=0)}{z+\dfrac{N(\vec{k},t=0)}{z+K(\vec{k})}}}=\frac{P_2(\vec{k},z)}{P_3(\vec{k},z)}, \tag{10}$$

where $P_n(\vec{k},z)$ denotes a real polynomial in $z$ of degree $n$. Making a partial fraction decomposition of this expression, and denoting by $z_i$ the roots of $P_3(\vec{k},z)$, which, by the way, are the same as the roots of $z+\tilde{M}(\vec{k},z)$, we have

$$\tilde{F}(\vec{k},z)=\sum_{i=1}^{3}\frac{A_i}{z-z_i}\Rightarrow F(\vec{k},t)=\sum_{i=1}^{3}A_i\exp[z_i t] \tag{11}$$

where the $z_i$ and the $A_i$ appear either as real or in complex conjugate pairs. Therefore either the three roots are real or one is real and the other two are a complex conjugate pair. In all practical situations the latter is the case, and then the roots are interpreted as describing a diffusive mode and a pair of damped propagating modes, much the same as in the hydrodynamic model, although for $k$ values outside this regime. The DSF is then a sum of three Lorentzian functions, one centered at $\omega=0$ which corresponds to the real root, and the other two centered at the imaginary parts of the complex conjugate pair.

At small $k$, the functional form of the dynamic magnitudes within the viscoelastic model coincides with that of the hydrodynamic model, which is known to be accurate in this region. Futhermore, the viscoelastic modes behave (as a function of $k$) much in the same way as the hydrodynamic modes. However, in spite of the previous similarities, there are basic differences between the viscoelastic and the hydrodynamic models. They are better understood if the derivation of both models is made by an alternative route using the generalized modes approach [5]. Here one considers the equations of motion of several dynamic magnitudes, namely, temperature (or energy) fluctuations, density fluctuations, current fluctuations, and stress tensor fluctuations. The viscoelastic model follows from considering couplings among the last three variables and ignoring their coupling with temperature fluctuations. The hydrodynamic model follows from considering couplings between the first three magnitudes and ignoring their coupling to the stress tensor fluctuations. A parameter quantifying the coupling between density and temperature fluctuations is the specific heat ratio $\gamma=C_p/C_v$. If $\gamma\sim 1$ the coupling is weak and the viscoelastic model is expected to be accurate; otherwise the model is expected to fail especially at small $k$.

Within the viscoelastic model, the analytical structure of the self-functions, i.e., $F_s(k,z)$, the SISF and the SDSF, is the same as that of the equivalent collective counterparts. However, the amplitude of the real coefficient associated with the real root is usually much greater than the amplitudes of the complex terms and therefore the associated propagating modes in the SDSF have often been neglected when the viscoelastic model has been applied to study the dynamic properties of one-component liquids. It may be argued whether these modes are real or a mere artifact of the model because the SDSF describe the one-particle behavior of the system. However, the close connection between collective and single particle properties in dense systems could induce the appearance of these modes. In any case, we stress that, to our knowledge, no detailed study of this possibility has yet been carried out.

### B. Binary system: Ashcroft-Langreth partials

The generalization of the foregoing formalism to binary systems is straightforward. We consider $N$ particles in a volume $V$ (therefore with number density $\rho=N/V$), composed of two species ($i=1,2$) which are characterized by the number of particles $N_i$, or concentration $x_i=N_i/N$, the atomic masses $m_i$, and ionic partial number densities $\rho_i=x_i\rho$. The interaction between particles of type $i$ and $j$ is described by effective interatomic pair potentials $\phi_{ij}(r)$ and the static structure by the partial pair distribution functions $g_{ij}(r)$.

We start from the Fourier transform of the partial microscopic number densities, defined as

$$\rho_{\vec{k}}^{(j)}(t)=\frac{1}{\sqrt{N_j}}\sum_{\ell=1}^{N_j}\exp[i\vec{k}\cdot\vec{r}_\ell^{(j)}(t)]\quad (j=1,2) \tag{12}$$

from which the partial intermediate scattering functions $F_{ij}(\vec{k},t)$ are obtained as

$$F_{ij}(\vec{k},t)=\langle\rho_{\vec{k}}^{(i)}(t)\rho_{-\vec{k}}^{(j)}(0)\rangle=[\mathbf{F}(\vec{k},t)]_{ij} \tag{13}$$

where the last equation defines the $2\times 2$ matrix $\mathbf{F}(\vec{k},t)$. The initial value of this matrix reduces to the matrix of Ashcroft-Langreth (AL) partial structure factors,

$$\mathbf{F}(\vec{k},t=0)=\mathbf{S}(\vec{k}), \tag{14}$$

where

$$[\mathbf{S}(\vec{k})]_{ij}=S_{ij}(\vec{k})=\delta_{ij}+(x_i x_j)^{1/2}\rho\int d\vec{r}\,[g_{ij}(r)-1]\exp[-i\vec{k}\cdot\vec{r}]. \tag{15}$$

As in the case of one-component systems, a similar separation into two terms is possible for all times, defining the self and distinct parts of the partial ISFs:

$$\mathbf{F}(\vec{k},t)=\mathbf{F}_{\boldsymbol{s}}(\vec{k},t)+\mathbf{F}_{\boldsymbol{d}}(\vec{k},t),$$

$$F_{ij}(\vec{k},t)=\delta_{ij}F_{s,j}(\vec{k},t)+(x_i x_j)^{1/2}F_{d,ij}(\vec{k},t). \tag{16}$$

Equations (3)–(8) remain formally the same, although now all the magnitudes in the equations are matrices, the products are to be understood as matrix products, and the exponent $-1$ means the matrix inverse. For instance, the memory function matrix obeys in the time and the Laplace domains the equations

$$\frac{d}{dt}\mathbf{F}(\vec{k},t) = -\int_0^t d\tau\, \mathbf{M}(\vec{k},\tau)\mathbf{F}(\vec{k},t-\tau), \tag{17}$$

$$\tilde{\mathbf{F}}(\vec{k},z) = [z\mathbf{I} + \tilde{\mathbf{M}}(\vec{k},z)]^{-1}\, \mathbf{F}(\vec{k},t=0), \tag{18}$$

where $\mathbf{I}$ is the unit matrix.

The matrices of frequency moments are given by [6]

$$[\omega^0(\vec{k})]_{ij} = S_{ij}(\vec{k}), \quad [\omega^2(\vec{k})]_{ij} = \delta_{ij}\, k^2 \frac{k_B T}{m_i}, \tag{19}$$

$$\begin{aligned}[\omega^4(\vec{k})]_{ij} &= \delta_{ij}\, k^2 \frac{k_B T}{m_i m_j}\left(3k^2 k_B T + \sum_\ell x_\ell \rho \int d\vec{r} g_{i\ell}(\vec{r}) \frac{\partial^2 \varphi_{i\ell}(\vec{r})}{\partial z^2}\right) \\ &\quad - (x_i x_j)^{1/2} k^2 \frac{k_B T}{m_i m_j}\rho \int d\vec{r} g_{ij}(\vec{r}) \cos(\vec{kr}) \frac{\partial^2 \varphi_{ij}(\vec{r})}{\partial z^2} \\ &= k^2 \frac{k_B T}{m_i m_j}\left[\delta_{ij}\left(3k^2 k_B T + \sum_\ell x_\ell \chi_{i\ell}(k)\right)\right. \\ &\quad \left. - (x_i x_j)^{1/2} \chi_{L;ij}(k)\right], \end{aligned} \tag{20}$$

where $T$ is the temperature, $k_B$ is Boltzmann's constant, $z$ denotes the direction of $\vec{k}$, and the last equality defines the functions $\chi_{ij}$ and $\chi_{L;ij}$.

The hierarchy of memory function matrices is again truncated at the third level, setting

$$\mathbf{K}(\vec{k},t) = \mathbf{K}(\vec{k})\delta(t) \Rightarrow \tilde{\mathbf{K}}(\vec{k},z) = \mathbf{K}(\vec{k}) \tag{21}$$

so that explicitly we have for the ISF matrix and the first and second order memory function matrices the relation (18) and

$$\tilde{\mathbf{M}}(\vec{k},z) = [z\mathbf{I} + \tilde{\mathbf{N}}(\vec{k},z)]^{-1}\, \mathbf{M}(\vec{k},t=0), \tag{22}$$

$$\tilde{\mathbf{N}}(\vec{k},z) = [z\mathbf{I} + \mathbf{K}(\vec{k})]^{-1}\, \mathbf{N}(\vec{k},t=0), \tag{23}$$

with the initial values of the memory function matrices given in terms of the frequency moments matrices as in Eqs. (7) and (8). In order to provide explicit expressions for the matrix elements of $\mathbf{K}(\vec{k})$ we follow Lovesey's arguments [3,4]. Setting $z=0$ in Eqs. (22) and (23) we have

$$\begin{aligned}\tilde{\mathbf{M}}(\vec{k},z=0) &= \tilde{\mathbf{N}}(\vec{k},z=0)^{-1}\, \mathbf{M}(\vec{k},t=0) \\ &= [\mathbf{K}(\vec{k})^{-1}\, \mathbf{N}(\vec{k},t=0)]^{-1}\, \mathbf{M}(\vec{k},t=0) \\ &= \mathbf{N}(\vec{k},t=0)^{-1}\, \mathbf{K}(\vec{k})\mathbf{M}(\vec{k},t=0) \end{aligned} \tag{24}$$

and therefore

$$\mathbf{K}(\vec{k}) = \mathbf{N}(\vec{k},t=0)\tilde{\mathbf{M}}(\vec{k},z=0)\mathbf{M}(\vec{k},t=0)^{-1}. \tag{25}$$

The value of $\tilde{\mathbf{M}}(\vec{k},z=0) = \int_0^\infty dt\, \mathbf{M}(\vec{k},t)$ is then assumed to be rather insensitive to the detailed shape of the $M_{ij}(\vec{k},t)$ and therefore a reasonable estimate can be obtained from an approximation that satisfies its correct short time behavior obtained by a simple Taylor expansion, namely,

$$\mathbf{M}(\vec{k},t) = \left(\mathbf{I} - \frac{t^2}{2}\mathbf{N}(\vec{k},t=0) + \cdots\right)\mathbf{M}(\vec{k},t=0). \tag{26}$$

The specific approximation we make for $\mathbf{M}(\vec{k},t)$ to perform the integral is

$$\mathbf{M}(\vec{k},t) \approx \exp\left(-\frac{t^2}{2}\mathbf{N}(\vec{k},t=0)\right)\mathbf{M}(\vec{k},t=0). \tag{27}$$

It is precisely at this point where the previous attempt to generalize the viscoelastic model [1] failed, since a similar approximation was made at the level of the matrix elements $M_{ij}(\vec{k},t)$ only, and not for the matrix $\mathbf{M}(\vec{k},t)$ itself, which is obviously wrong because we are dealing with matrix products.

Within this approximation $\tilde{\mathbf{M}}(\vec{k},z=0)$ would be given by the time integral of the exponential function times the matrix $\mathbf{M}(\vec{k},t=0)$. Trying to correct the inaccuracies that might have been introduced by this approximation, this value is premultiplied by a matrix $\Xi$ of constants to be determined later. In this way an explicit expression for $\mathbf{K}(\vec{k})$ is found in terms of the initial values of the second order memory functions:

$$\mathbf{K}(\vec{k}) = \mathbf{N}(\vec{k},t=0)\Xi \int_0^\infty dt\, \exp\left(-\frac{t^2}{2}\mathbf{N}(\vec{k},t=0)\right). \tag{28}$$

The determination of $\Xi$ is carried out by imposing that in the free-particle limit ($k\to\infty$) the dynamic structure factor matrix evaluated at zero frequency recovers the exact free-gas result, i.e.,

$$[\mathbf{S}(\vec{k},\omega=0)]_{ij} = \delta_{ij}\left(\frac{1}{2\pi k^2}\frac{m_i}{k_B T}\right)^{1/2} \tag{29}$$

leading to the result $\Xi = (2\sqrt{2}/\pi)\mathbf{I}$. In the Appendix we give details of this derivation and explicit expressions for the matrix elements of $\mathbf{K}(\vec{k})$.

Turning now to the analytic behavior of $\tilde{\mathbf{F}}(\vec{k},z)$ we see in Eq. (18) that it is determined by the inverse of the matrix $[z\mathbf{I}+\tilde{\mathbf{M}}(\vec{k},z)]$, namely, the transpose of the adjoint divided by the determinant. Therefore, all the $\tilde{F}_{ij}(k,z)$ have the same analytic behavior, which is determined by the solutions of the equation

$$\det[z\mathbf{I} + \tilde{\mathbf{M}}(\vec{k},z)] = 0. \tag{30}$$

As in the one-component case, this determinant is a real rational function, whose form is obtained by writing down explicitly the equations for the memory function matrices up to the third, leading now to an expression of the type $P_6(\vec{k},z)/P_4(\vec{k},z)$. Consequently there will be six roots, which in principle may appear (together with the corresponding amplitude matrices) as six real values, four real values and a complex conjugate pair, two real values and two complex conjugate pairs, or three complex conjugate pairs. Therefore we have

$$\tilde{\mathbf{F}}(\vec{k},z)=\sum_{i=1}^{6}\frac{1}{z-z_i}\mathbf{A}_i,\quad \mathbf{F}(\vec{k},t)=\sum_{i=1}^{6}\mathbf{A}_i\exp[z_i t], \tag{31}$$

where the $\mathbf{A}_i$ are the $\vec{k}$-dependent $2\times 2$ amplitude matrices. In the actual calculations made for liquid Li-Na [2], as well as those carried out in this paper, we found for all $k$ two real roots and two pairs of complex conjugate roots, at variance with some other calculations where one of the complex conjugate pair transforms into two real roots below a certain small $k$ value [7,8]. All roots have negative real parts [7], so we can rewrite the previous equation as

$$\tilde{F}_{ij}(\vec{k},z)=\frac{A_{ij}}{z-z^{(1)}}+\frac{A_{ij}^{*}}{z-z^{(1)*}}+\frac{B_{ij}}{z-z^{(2)}}+\frac{B_{ij}^{*}}{z-z^{(2)*}}+\frac{C_{ij}}{z+z^{(3)}}+\frac{D_{ij}}{z+z^{(4)}}, \tag{32}$$

where the $\vec{k}$-dependent coefficients $A_{ij}$ and $B_{ij}$ are complex, while $C_{ij}$ and $D_{ij}$ are real. The complex roots $z^{(j)}(k)=-\Gamma^{(j)}(k)\pm i\omega_s^{(j)}(k)(j=1,2)$ describe propagation, where the real part $\Gamma^{(j)}(k)$ represents damping whereas the imaginary part $\omega_s^{(j)}(k)$ represents the propagation. A set of two complex conjugate roots represents propagation in opposite directions. The real roots $-z^{(j)}(k)(j=3,4)$ stand for purely diffusive processes. Out of the six roots, only four go to zero when $k\to 0$; this coincides with the behavior of the four hydrodynamic roots predicted by the hydrodynamic equations for binary mixtures. Again we stress that although the small $k$ behavior of the four viscoelastic modes is similar to the hydrodynamic ones, there are quantitative differences between them based on the same reason as in the one-component case, namely, the neglect of coupling with the energy fluctuations. As in one-component liquids, the viscoelastic model is expected to work for systems where this coupling is weak, i.e., those with specific heat ratio $\gamma\sim 1$. The other two viscoelastic roots have a finite value when $k\to 0$, while the corresponding amplitudes vanish in this limit; this is the typical behavior of kinetic modes. The six roots lead to a $S_{ij}(k,\omega)$ given as a sum of six Lorentzians, two centered at $\omega=0$ and the other four at $\omega=\pm\omega_s^{(j)}(k)(j=1,2)$.

### C. Binary system: Bhatia-Thornton partials

An alternative description of the structure of binary alloys is provided by the so called Bhatia-Thornton (BT) functions. The BT static partial structure factors, namely, number-number $S_{NN}(k)$, number-concentration $S_{Nc}(k)$, and concentration-concentration $S_{cc}(k)$ partial structure factors, describe the correlations among fluctuations in number density (irrespective of chemical composition) and concentration density, and are linear combinations of the AL partial structure factors $S_{ij}(k)$. These relations are most compactly written if one defines the matrix $\mathcal{S}(k)$ of modified BT partial structure factors in terms of the matrix $\mathbf{S}(k)$ of AL partial structure factors:

$$\mathcal{S}=\mathbf{X}\,\mathbf{S}\,\mathbf{X} \tag{33}$$

where

$$\mathcal{S}(k)=\begin{pmatrix} S_{NN}(k) & S_{Nc}(k)/(x_1x_2)^{1/2} \\ S_{cN}(k)/(x_1x_2)^{1/2} & S_{cc}(k)/(x_1x_2)\end{pmatrix} \tag{34}$$

and

$$\mathbf{X}=\mathbf{X}^{-1}=\begin{pmatrix}\sqrt{x_1} & \sqrt{x_2}\\ \sqrt{x_2} & -\sqrt{x_1}\end{pmatrix}.$$

All other BT magnitudes (intermediate scattering functions, first, second and third memory functions, frequency moments, etc.) are defined in the same way, pre- and post-multiplying the corresponding matrix of AL magnitudes by the matrix $\mathbf{X}$; for instance, the BT partial ISFs are defined by the matrix $\mathcal{F}(\vec{k},t)$,

$$\mathcal{F}(\vec{k},t)=\mathbf{X}\,\mathbf{F}(\vec{k},t)\mathbf{X}=\mathcal{F}_s(\vec{k},t)+\mathcal{F}_d(\vec{k},t), \tag{35}$$

which leads to (dropping the arguments of the functions)

$$F_{NN}=\{x_1F_{s,1}+x_2F_{s,2}\}+\{x_1^2F_{d,11}+2x_1x_2F_{d,12}+x_2^2F_{d,22}\}, \tag{36}$$

$$\frac{F_{Nc}}{(x_1x_2)^{1/2}}=\{(x_1x_2)^{1/2}(F_{s,1}-F_{s,2})\}+\{(x_1x_2)^{1/2}[x_1(F_{d,11}-F_{d,12})+x_2(F_{d,12}-F_{d,22})]\}, \tag{37}$$

and

$$\frac{F_{cc}}{x_1x_2}=\{x_2F_{s,1}+x_1F_{s,2})+\{x_1x_2[F_{d,11}-2F_{d,12}+F_{d,22})], \tag{38}$$

where the first braces in each equation enclose the BT SISFs and the second braces enclose the BT distinct ISFs.

The viscoelastic model for the BT functions is then defined by the relations

$$\tilde{\mathcal{F}}(\vec{k},z)=[z\mathbf{I}+\tilde{\mathcal{M}}(\vec{k},z)]^{-1}\mathcal{F}(\vec{k},t=0), \tag{39}$$

$$\tilde{\mathcal{M}}(\vec{k},z)=[z\mathbf{I}+\tilde{\mathcal{N}}(\vec{k},z)]^{-1}\mathcal{M}(\vec{k},t=0), \tag{40}$$

$$\tilde{\mathcal{N}}(\vec{k},z)=[z\mathbf{I}+\mathcal{K}(\vec{k})]^{-1}\mathcal{N}(\vec{k},t=0), \tag{41}$$

$$\mathcal{K}(\vec{k})=\mathcal{N}(\vec{k},t=0)\Xi\int dt\,\exp\left(-\frac{t^2}{2}\mathcal{N}(\vec{k},t=0)\right), \tag{42}$$

$$\mathcal{F}(\vec{k},t=0)=\Omega^0(\vec{k})=\mathcal{S}(k), \tag{43}$$

$$\mathcal{M}(\vec{k},t=0)=\Omega^2(\vec{k})\Omega^0(\vec{k})^{-1}, \tag{44}$$

$$\mathcal{N}(\vec{k},t=0)=\Omega^4(\vec{k})\Omega^2(\vec{k})^{-1}-\Omega^2(\vec{k})\Omega^0(\vec{k})^{-1}, \tag{45}$$

$$\Omega^n(\vec{k})=\mathbf{X}\,\omega^n(\vec{k})\mathbf{X}, \tag{46}$$

or explicitly

$$\Omega_{NN}^2=k^2k_BT\left(\frac{x_1}{m_1}+\frac{x_2}{m_2}\right),$$

$$\Omega_{cc}^2 = k^2 k_B T\left(\frac{x_1}{m_2} + \frac{x_2}{m_1}\right),$$

$$\Omega_{Nc}^2 = k^2 k_B T (x_1 x_2)^{1/2}\left(\frac{1}{m_1} - \frac{1}{m_2}\right) \tag{47}$$

and

$$\frac{\Omega_{NN}^4}{k^2 k_B T} = \left(\frac{x_1}{m_1^2} + \frac{x_2}{m_2^2}\right)3k^2 k_B T + x_1 x_2\left(\frac{1}{m_2} - \frac{1}{m_1}\right)^2 \chi_{12} + \left(\frac{x_1^2}{m_1^2}(\chi_{11} - \chi_{L;11}) + 2\frac{x_1 x_2}{m_1 m_2}(\chi_{12} - \chi_{L;12}) + \frac{x_2^2}{m_2^2}(\chi_{22} - \chi_{L;22})\right),$$

$$\frac{\Omega_{cc}^4}{k^2 k_B T} = \left(\frac{x_1}{m_2^2} + \frac{x_2}{m_1^2}\right)3k^2 k_B T + \left(\frac{x_1}{m_2} + \frac{x_2}{m_1}\right)^2 \chi_{12} + x_1 x_2\left(\frac{1}{m_1^2}(\chi_{11} - \chi_{L;11}) - \frac{2}{m_1 m_2}(\chi_{12} - \chi_{L;12}) + \frac{1}{m_2^2}(\chi_{22} - \chi_{L;22})\right),$$

$$\frac{\Omega_{Nc}^4}{k^2 k_B T (x_1 x_2)^{1/2}} = \left(\frac{1}{m_1^2} - \frac{1}{m_2^2}\right)3k^2 k_B T + x_1\left(\frac{\chi_{11}}{m_1^2} - \frac{\chi_{12}}{m_2^2}\right) + x_2\left(\frac{\chi_{12}}{m_1^2} - \frac{\chi_{22}}{m_2^2}\right) - x_1\left(\frac{\chi_{L;11}}{m_1^2} - \frac{\chi_{L;12}}{m_1 m_2}\right) - x_2\left(\frac{\chi_{L;12}}{m_1 m_2} - \frac{\chi_{L;22}}{m_2^2}\right). \tag{48}$$

### D. Reduction to the one-component case

In the case of a pseudobinary mixture, when all the particles are of the same type but are labeled differently, all the partial pair distribution functions reduce to that of the real one-component liquid, i.e., $g_{11}(r) = g_{22}(r) = g_{12}(r) = g(r)$. However, the AL partial structure factor, do not coincide with that of the real one-component system $S(k)$, but

$$S_{ij}(k) = \delta_{ij} + (x_i x_j)^{1/2}[S(k) - 1].$$

Explicitly we have

$$S_{11}(k) = x_2 + x_1 S(k),$$

$$S_{22}(k) = x_1 + x_2 S(k),$$

$$S_{12}(k) = -(x_1 x_2)^{1/2} + (x_1 x_2)^{1/2} S(k). \tag{49}$$

The BT partial structure factors, on the other hand, behave more simply, because we now have $S_{NN}(k) = S(k)$, $S_{Nc}(k) = 0$, and $S_{cc}(k)/(x_1 x_2) = 1$.

In many one-component systems (in particular liquid metals near the triple point) the value of $S(k)$ for small $k$ is rather small, of the order $(2-3)\times 10^{-2}$, reflecting a small value of the isothermal compressibility. For a pseudobinary system, we therefore obtain that, except for very dilute mixtures, the small $k$ values of the partial static structure factors are dominated by the first terms of Eqs. (49), which take on significantly higher values than that of the structure factor of the one-component liquid.

The situation concerning the ISFs is similar. According to their definition [see Eq. (16)], we have $F_{s,1}(\vec{k},t) = F_{s,2}(\vec{k},t) = F_s(\vec{k},t)$, which is the SISF of the real one-component liquid, and $F_{d,11}(\vec{k},t) = F_{d,22}(\vec{k},t) = F_{d,12}(\vec{k},t) = F_d(\vec{k},t)$, which is the distinct ISF of the real one-component liquid. Therefore the AL partial ISFs are given by

$$F_{ij}(\vec{k},t) = \delta_{ij} F_s(\vec{k},t) + (x_i x_j)^{1/2} F_d(\vec{k},t),$$

and explicitly

$$F_{11}(\vec{k},t) = x_2 F_s(\vec{k},t) + x_1 F(\vec{k},t),$$

$$F_{22}(\vec{k},t) = x_1 F_s(\vec{k},t) + x_2 F(\vec{k},t),$$

$$F_{12}(\vec{k},t) = -(x_1 x_2)^{1/2} F_s(\vec{k},t) + (x_1 x_2)^{1/2} F(\vec{k},t), \tag{50}$$

which is an awkward relation that induces a behavior of the partial ISFs very different from that of the real one-component liquid. On the other hand the BT partial ISFs become

$$F_{NN}(\vec{k},t) = (x_1 + x_2)F_s(\vec{k},t) + (x_1 + x_2)^2 F_d(\vec{k},t) = F_s(\vec{k},t) + F_d(\vec{k},t) = F(\vec{k},t), \tag{51}$$

$$F_{Nc}(\vec{k},t) = 0, \tag{52}$$

$$F_{cc}(\vec{k},t)/(x_1 x_2) = (x_1 + x_2)F_s(\vec{k},t) = F_s(\vec{k},t), \tag{53}$$

that is, the cross function vanishes, the number-number function reduces to the ISF of the real one-component liquid, and the concentration-concentration function, properly normalized, reduces to the SISF of the real one-component system.

Coming to the viscoelastic model, in particular in the BT formulation, we note that all the magnitudes are determined by the frequency moment matrices. In a pseudobinary system we have $m_1 = m_2$, and all the $\chi_{ij}$ reduce to $\chi$ which is obtained by setting $g_{ij}(r) = g(r)$ and $\phi_{ij}(r) = \phi(r)$; also by the same procedure, all the $\chi_{L;ij}$ reduce to $\chi_L$. Then all the frequency moment matrices in the BT formulation become diagonal, and therefore the same occurs to all the other matrices, so that the matrix operations in fact become the same operations on the diagonal elements of the matrices, i.e., the *NN* and the *cc* functions.

In particular we have

$$\Omega_{NN}^4 = \frac{k^2 k_B T}{m^2}[3k^2 k_B T + \chi(k) - \chi_L(k)] \tag{54}$$

$$\Omega_{cc}^4 = \frac{k^2 k_B T}{m^2}[3k^2 k_B T + \chi(k)] \tag{55}$$

which are, respectively, the fourth frequency moments of the DSF and the SDSF of the one-component system. Likewise

$$\Omega_{NN}^2 = \frac{k^2 k_B T}{m} = \Omega_{cc}^2, \tag{56}$$

which again are the second frequency moments of the DSF and the SDSF of the one-component system, and as we stated before $\Omega_{NN}^0 = S_{NN}(k) = S(k)$ and $\Omega_{cc}^0 = S_{cc}(k)/(x_1 x_2) = 1$, which are the corresponding zeroth frequency moments of the DSF and the SDSF of the one-component system, respectively.

Therefore, the present formulation of the viscoelastic model for the collective dynamic properties of binary mixtures recovers, in the case of a pseudobinary system, not only the viscoelastic model for the collective properties of the underlying one-component system, through the number-number BT functions, but also the viscoelastic model for its single particle properties, through the concentration-concentration functions. Moreover, the determinant that leads to the different modes factorizes into two terms, one that includes the modes of the DSF with the other term accounting for the modes of the SDSF of the one-component system; this implies that both sets of modes are decoupled.

## III. RESULTS

In this section we study three systems and compare the results of the viscoelastic model with those obtained by molecular dynamics simulations.

The first is a pseudobinary system, in which all particles are in fact the same type, but half of them are labeled as 1 and the other half as 2 ($x_1 = x_2 = 0.5$). Specifically the system is representative of $^7$Li at $T = 725$ K and $\rho = 0.042$ Å$^{-3}$, and the effective pair potentials used (all three identical) were obtained using the empty core pseudopotential [9], with core radius 1.44 Å. Some MD results for this system have been reported elsewhere [10] and are extended here. They have been obtained using 668 particles in a cubic box with periodic boundary conditions.

The other two cases correspond to two Li-based alloys, $Li_{0.7}Mg_{0.3}$, which is a typical quasi-ideal mixture, and $Li_4Pb$, which is a reference case for a class of compound forming alloys with preionic ordering. The temperatures and densities are $T = 887$ K and $\rho = 0.040\,711$ Å$^{-3}$ for $Li_{0.7}Mg_{0.3}$ and $T = 1085$ K and $\rho = 0.045\,58$ Å$^{-3}$ for $Li_4Pb$. The interatomic pair potentials were obtained in the case of $Li_{0.7}Mg_{0.3}$ within the neutral pseudoatom method [11] while in the case of $Li_4Pb$ they were taken from Copestake *et al.* [12]. The collective propeties of the $Li_{0.7}Mg_{0.3}$ alloy have been studied by Anento and Padró [13,14], and those of $Li_4Pb$ by several authors [15,16], the latter being the first system where the fast sound phenomenon was observed, which consists in the appearance of a peak in the Li-Li dynamic structure factor, absent in the Pb-Pb one, with a very high frequency similar to that of pure Li. In this paper we include MD results obtained for both systems, in the case of $Li_{0.7}Mg_{0.3}$ with 570 particles and in the case of $Li_4Pb$ with 600 particles for most $k$ values and with 11 000 particles for the smallest ones ($k_{\min} = 0.10$ Å$^{-1}$).

The difference between the AL ISFs of the two types of system is striking: while $Li_4Pb$ has $F_{ij}(k,t)$, and in particular the Li-Li partial, that decay more or less rapidly with time, similar to the behavior of one-component systems, $Li_{0.7}Mg_{0.3}$ on the other hand shows $F_{ij}(k,t)$ which have much larger magnitudes and decay much more slowly, in practice making very difficult the Fourier transformation that leads to the DSFs.

A proper description of such different behaviors, along with the case already studied of phase separating systems like $Li_{0.69}Na_{0.31}$ [2], would therefore provide reliability to the viscoelastic model.

The static structure and the frequency moments, which are a required input of the viscoelastic model for the calculation of the dynamic properties, have been computed using the variational modified hypernetted chain (VMHNC) approximation [17] which reproduces rather well the simulation results, although small differences can and do appear in the structural functions, which show up, for instance, in a small mismatch of the initial theoretical and simulation values of the ISFs. While it would be possible to use the simulated $S_{ij}(k)$ instead of the VMHNC ones, the calculation by simulation of the fourth frequency moments is rather unreliable.

We recall that the viscoelastic model is expected to be accurate for systems with $\gamma \sim 1$. Generalized hydrodynamics calculations of $\gamma$ have been performed for liquid Li [18], liquid Pb [19], and liquid Na-K and K-Cs alloys [20], leading in all cases to $\gamma$ values not far from 1. These results give some support to the application of the viscoelastic model to liquid metals and alloys, in contrast to other systems like Lennard-Jones liquids [7,8] where $\gamma$ is larger.

### A. Model 1: Pseudobinary system

Due to the particular concentration $x_1 = x_2 = 0.5$, an additional symmetry appears in the system, that implies that $S_{11}(k) = S_{22}(k)$, $F_{11}(k,t) = F_{22}(k,t)$ and so on.

Figure 1 shows the partial structure factors obtained from the simulation and the VMHNC theory, which are practically coincident. The first thing to note is that, as stated above, the small $k$ values attained by the $S_{ij}(k)$ are in magnitude close to 0.5 (the concentrations) which is one order of magnitude larger than the structure factor of the corresponding one-component system in the same region. This will imply a much larger initial value of the partial ISFs of the system as compared to the ISF of the one-component system. The $F_{ij}(k,t)$ are shown in Fig. 2, where we have plotted both the MD results and the viscoelastic ones. The results for small $k$ are markedly different from the $F(k,t)$ of the one-component system, and not only in the initial value. The latter shows clear oscillations around zero, whereas the partial ISFs of the pseudobinary system show a large diffusive component which decays very slowly.

The reason for this behavior can be found in the roots and corresponding amplitudes that are obtained within the vis-

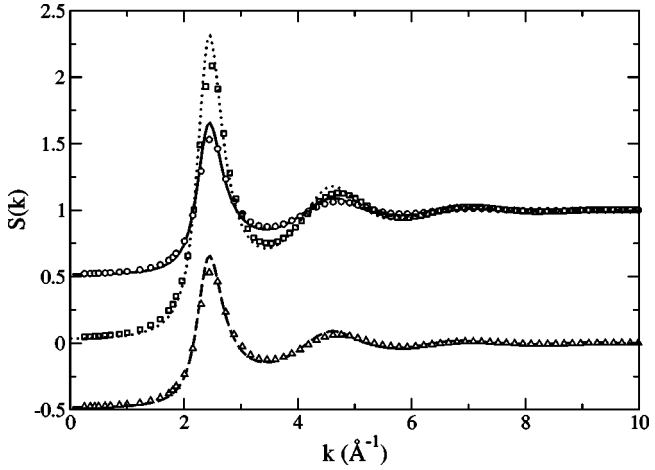


FIG. 1. Static partial structure factors for pseudobinary Li. Full line and circles, $S_{11}(k)=S_{22}(k)$; dashed line and triangles, $S_{12}(k)$; dotted line and squares, one-component system $S(k)$. The lines are theoretical results and the symbols denote MD simulation results.

coelastic model. The roots are plotted in Fig. 3, where we see that one of the propagating roots vanishes in the $k=0$ limit, while the other remains nonzero in this limit. We recall that in a pseudobinary system the determinant that leads to the roots factors into two third degree polynomials, which correspond to the modes of the DSF and the SDFS of the one-component system respectively. The first propagating root corresponds to the propagating mode in the DSF of the one-component system, while the nonvanishing root is an unexpected propagating mode that appears in the SDSF of the one-component system. Of the remaining two real roots, the largest one in magnitude for small $k$ is the diffusive mode of the DSF of the one-component system, whereas the smallest one in magnitude corresponds to the diffusive mode of the SDSF of the one-component system. It is precisely this last root that is responsible for the behavior of the partial $F_{ij}(k,t)$,

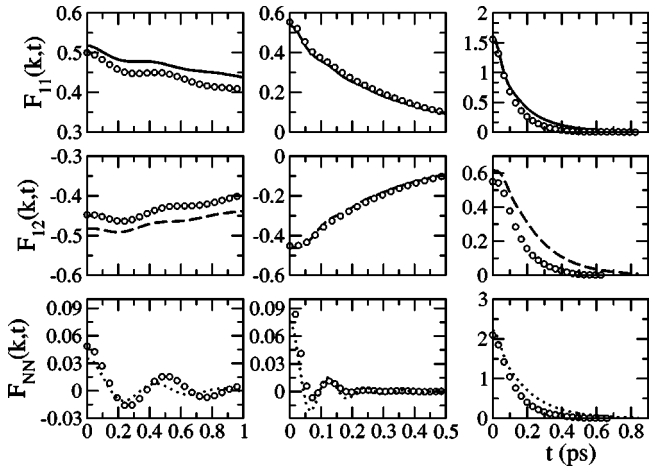


FIG. 2. Partial ISFs for pseudobinary Li. Full lines (top panel), $F_{11}(k,t)=F_{22}(k,t)$, dashed line (middle panel), $F_{12}(k,t)$; dotted line (bottom panel), $F_{NN}(k,t)$, which coincides with the one-component system $F(k,t)$. The symbols are the corresponding MD results. Left column, $k=0.23$ Å$^{-1}$; middle column, $k=1.23$ Å$^{-1}$; right column, $k=2.51$ Å$^{-1}$.

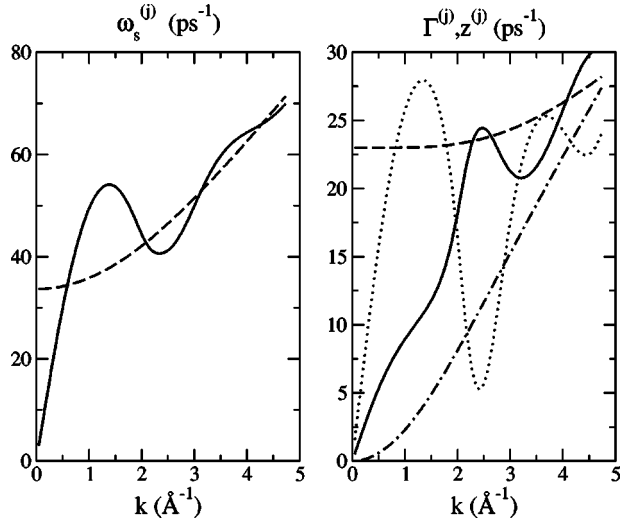


FIG. 3. Roots of pseudobinary Li in the viscoelastic model. Full lines, $\omega_s^{(1)}$ and $\Gamma^{(1)}$; dashed lines, $\omega_s^{(2)}$ and $\Gamma^{(2)}$; dotted line, $z^{(3)}$; dash-dotted line, $z^{(4)}$.

since its contribution is the most slowly decaying one. Moreover its amplitude is the largest for small $k$, as can be observed in Fig. 4. In fact we have plotted only the amplitudes corresponding to the 11 partial, since due to the symmetry imposed by the concentrations the amplitudes corresponding to the 22 partial are the same as the 11 ones, while we also have that $A_{12}=A_{11}$, $B_{12}=-B_{11}$, $C_{12}=C_{11}$, $D_{12}=-D_{11}$. Note that $B_{11}$ goes to 0 as $k\rightarrow 0$, which is another characteristic feature of the kinetic modes. It is also interesting to observe the similarity between $C_{11}$ and the structure factors. We can therefore conclude that the extremely slow decay of $F_{ij}(k,t)$ is a direct consequence of the influence of the single particle dynamics on the behavior of the ISFs, and this is due to the very definition of the AL partial ISFs. When one comes tothe BT partials no such problems arise, since there is a complete decoupling of the single particle dynamics, which goes ex-

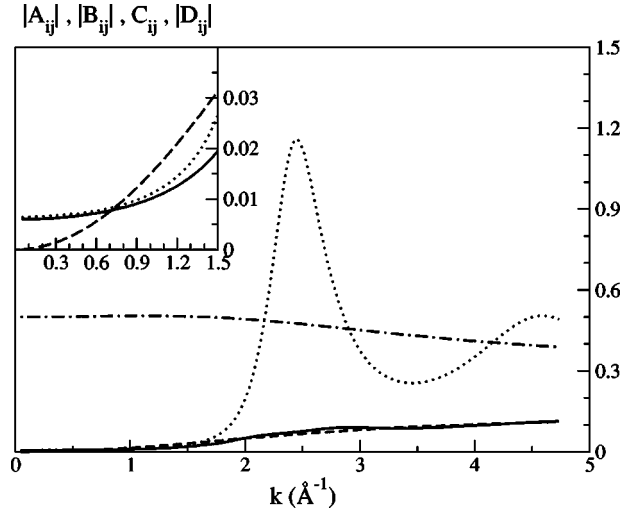


FIG. 4. Amplitudes of the different modes of pseudobinary Li in the viscoelastic model. Full lines, $A_{11}$; dashed lines, $B_{11}$; dotted lines, $C_{11}$; dash-dotted line, $D_{11}$.

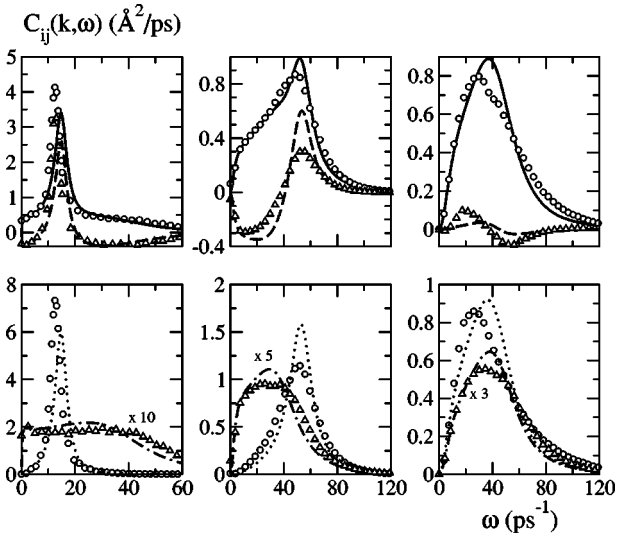


FIG. 5. Partial currents for pseudobinary Li. Lines are theoretical results and symbols denote simulation data. Full line and circles (upper panel), $C_{11}(k,\omega)=C_{22}(k,\omega)$; dashed line and triangles (upper panel), $C_{12}(k,\omega)$; dotted line and circles (lower panel), $C_{NN}(k,\omega)$, which coincides with the one-component system $C(k,\omega)$; dash-dotted line and triangles (lower panel), scaled $C_{cc}(k,\omega)$, which coincides with the one-component system $C_s(k,\omega)$. Left column, $k=0.23$ Å$^{-1}$; middle column, $k=1.23$ Å$^{-1}$; right column, $k=2.18$ Å$^{-1}$.

clusively into the concentration-concentration partial, and the collective dynamics, which is exclusively responsible for the number-number partial. Obviously this complete decoupling is due to the ideal character of this system.

The Fourier transforms of the longitudinal current correlation functions are directly related to the DSFs, through the relation $C_{ij}(k,\omega)=(\omega^2/k^2)S_{ij}(k,\omega)$ (and the same relation for the BT currents), while they can be calculated independently in the MD runs. They are especially useful in the cases where a slowly decaying term appears in the ISFs which complicates the computation of the DSFs, while the multiplication by $\omega^2$ depletes the low frequency modes and enhances the high frequency ones. In Fig. 5 we show the functions $C_{ij}(k,\omega)$ and also the BT ones. We always find a clear peak and a minimum in $C_{12}(k,\omega)$, while there is a clear maximum in $C_{11}(k,\omega)$ at the position of the peak of $C_{12}(k,\omega)$, and sometimes a shoulder at the position of the minimum. These are of course the remnants of the two propagating modes. The coincidence of the shoulder of $C_{11}(k,\omega)$ with the minimum of $C_{12}(k,\omega)$ suggests that the second propagating mode on top of being kinetic is optical in character, with the two "species" moving in opposite directions. The appearance of an optical mode in a pseudobinary liquid system resembles a similar effect that appears for crystals: when a linear chain with equilibrium distance $a$ is considered as a chain with equilibrium distance $2a$ with a basis formed by two "different" atoms separated by a distance $a$ [21], then the first Brillouin zone becomes half the original one, and the original dispersion relation becomes folded into the new one leading to the optical mode. The BT currents on the other hand always show a single peak, in the *NN* case (which is the current of the one-component system) at the positions of the peaks in the 11 and 12 functions, and in the *cc* case (which is the self-current of the one-component system) at the position of the minimum of the 12 function.

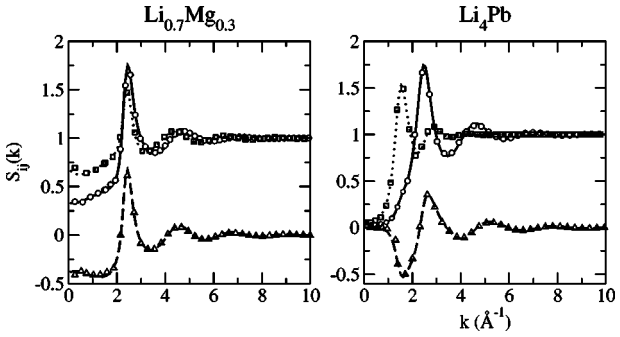


FIG. 6. Static partial structure factors for $Li_{0.7}Mg_{0.3}$ and $Li_4Pb$. Full lines and circles, $S_{11}(k)$; dotted lines and squares, $S_{22}(k)$; dashed lines and triangles, $S_{12}(k)$. The lines are theoretical results and the symbols denote MD simulation results.

The appearance of the peak in the self-currents of the one-component system is very clear in the MD simulations, showing that also in the single particle properties of this system there are indeed propagating contributions, of kinetic character. These modes had not been reported previously, at least to our knowledge, since the focus has usually been put on the initial value and the width of the SDSF of the systems, analyzing the behavior of these properties within the different theoretical approaches. The reproduction of these propagating modes by the viscoelastic model (for the single particle properties) is therefore an interesting property of this theory, and warrants a wider application of the model in the analysis of the single-particle properties of, at least, this type of dense liquids.

### B. Li-based alloys: Ideal and compound forming mixtures

In the following we will denote Li as component 1. The partial static structure factors of both liquid alloys are shown in Fig. 6. Those corresponding to $Li_{0.7}Mg_{0.3}$ are similar in character to those of the pseudobinary alloy, except for the difference in concentration, so the values of $S_{ij}(k=0)$ are larger than that of a one-component system. On the other hand the results for $Li_4Pb$ are very different; in particular, the values of $S_{ij}(k=0)$ are all three similar in magnitude to the case of a one-component system; moreover the dip in $S_{12}(k)$ and the coincident positions of the maximum of $S_{11}(k)$ and the minimum of $S_{22}(k)$ are indicative of a kind of ionic ordering in the melt [22]. The corresponding ISFs are also strikingly different for the two systems, especially for small $k$, as observed in Figs. 7 and 8. As in the pseudobinary system, the ISFs of $Li_{0.7}Mg_{0.3}$ have a very slowly decaying diffusive term for small $k$. In the case of $Li_4Pb$, the slowly decaying term is practically absent in $F_{11}(k,t)$ and while there is indeed such a term in $F_{12}(k,t)$ and especially in $F_{22}(k,t)$, it decays much more rapidly than in $Li_{0.7}Mg_{0.3}$ (observe the $y$-axis scales in Figs. 7 and 8) even though the Pb ionic mass is much larger than the Mg one.

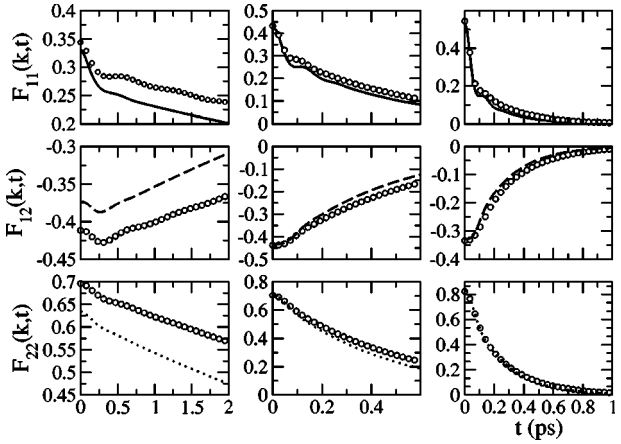


FIG. 7. Partial ISFs for $Li_{0.7}Mg_{0.3}$. Lines are theoretical results and symbols are simulation data. Full lines (top panel), $F_{11}(k,t)$; dashed lines (middle panel), $F_{12}(k,t)$; dotted lines (bottom panel), $F_{22}(k,t)$. Left column, $k=0.28$ Å$^{-1}$ (theory), 0.26 Å$^{-1}$ (simulation); middle column, $k=1.25$ Å$^{-1}$ (theory), 1.23 Å$^{-1}$ (simulation); right column, $k=1.88$ Å$^{-1}$ (theory and simulation).

Again the reason for such behaviors can be traced back to the roots and the amplitudes of the modes associated with the three partials. The roots are shown in Fig. 9. We see that, due to the mass difference, the frequency $\omega_s^{(1)}$ and damping $\Gamma^{(1)}$ of the low frequency root are larger for $Li_{0.7}Mg_{0.3}$ than for $Li_4Pb$, while the high frequency root and the larger real root have quite similar magnitude and variation with $k$ for the two systems, being much more influenced by the masses of the components and the thermodynamic state than by the particular structure of the alloy. The smallest real root $z^{(4)}$ also behaves differently for $Li_{0.7}Mg_{0.3}$ and $Li_4Pb$, staying much closer to $\Gamma^{(1)}$ for the latter. For small $k$, in particular, $z^{(4)}$ is significantly larger for $Li_4Pb$ than for $Li_{0.7}Mg_{0.3}$, which explains the faster decay of $F_{12}(k,t)$ and $F_{22}(k,t)$ in $Li_4Pb$.

Figures 10–12 show the amplitudes for $F_{ij}(k,t)$. The first noticeable feature is that the $F_{22}(k,t)$ functions are completely dominated for all $k$ by the smallest real root, and to a lesser extent by the low frequency root, the other two amplitudes being smaller, except in the case of $Li_{0.7}Mg_{0.3}$ in the region of the main peak of the corresponding structure factor and for small $k$, where the amplitude corresponding to the larger real root is also significant. The case of the $F_{12}(k,t)$ functions is rather similar, with the difference that for small $k$ in $Li_{0.7}Mg_{0.3}$ the three amplitudes corresponding to the two propagating roots and the larger real root are of similar magnitude. Note again the striking similarity between the amplitudes of the smallest real root and the structure factors, with $D_{12}$ and $D_{22}$ following, respectively, $S_{12}(k)$ and $S_{22}(k)$. The different behavior of these structure factors for the two systems implies now that the amplitude of the diffusive mode is much smaller for $Li_4Pb$ than for $Li_{0.7}Mg_{0.3}$. As for the $F_{11}(k,t)$ functions, the structure of the amplitudes is richer.

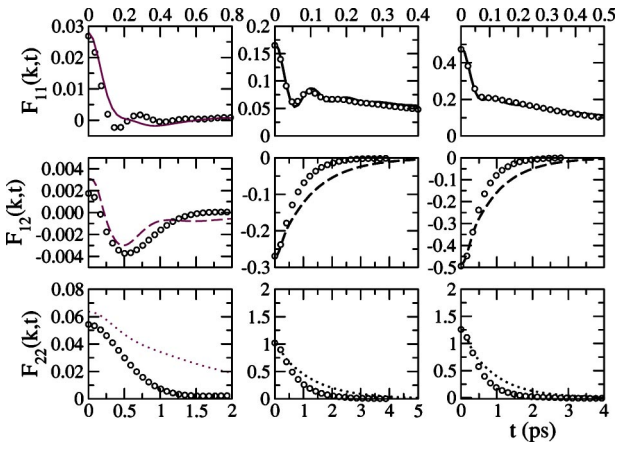


FIG. 8. Partial ISFs for $Li_4Pb$. The meanings of the lines and symbols are the same as in the previous figure. Left column, $k=0.31$ Å$^{-1}$ (theory), 0.27 Å$^{-1}$ (simulation); middle column, $k=1.30$ Å$^{-1}$ (theory and simulation); right column, $k=1.76$ Å$^{-1}$ (theory), 1.74 Å$^{-1}$ (simulation). Note the different scales in the time axis for $F_{11}(k,t)$.

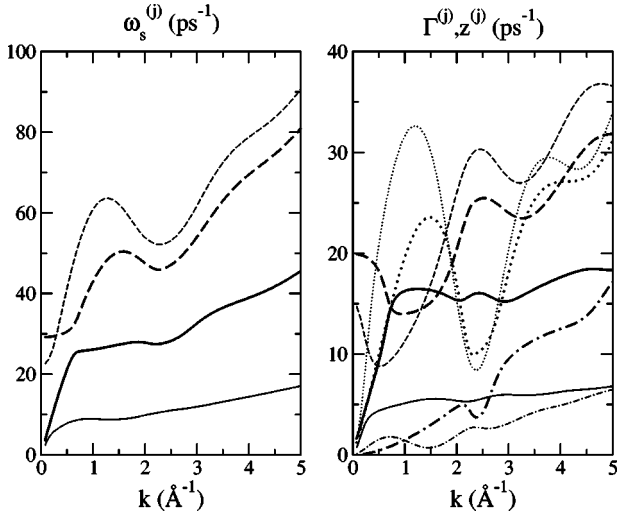


FIG. 9. Roots of $Li_{0.7}Mg_{0.3}$ (thick lines) and $Li_4Pb$ (thin lines) in the viscoelastic model. Full lines, $\omega_s^{(1)}$ and $\Gamma^{(1)}$; dashed lines, $\omega_s^{(2)}$ and $\Gamma^{(2)}$; dotted lines, $z^{(3)}$; dash-dotted lines, $z^{(4)}$.

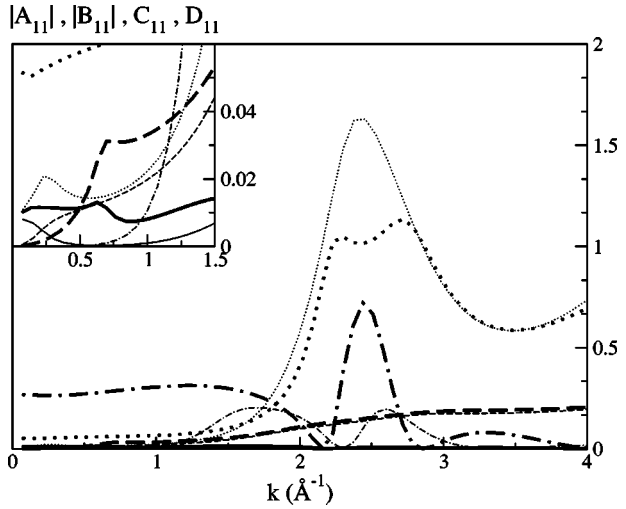


FIG. 10. Amplitudes of the different modes of $F_{11}(k,t)$ for $Li_{0.7}Mg_{0.3}$ (thick lines) and $Li_4Pb$ (thin lines) in the viscoelastic model. Full lines, $A_{11}$; dashed lines, $B_{11}$; dotted lines, $C_{11}$; dash-dotted lines, $D_{11}$.

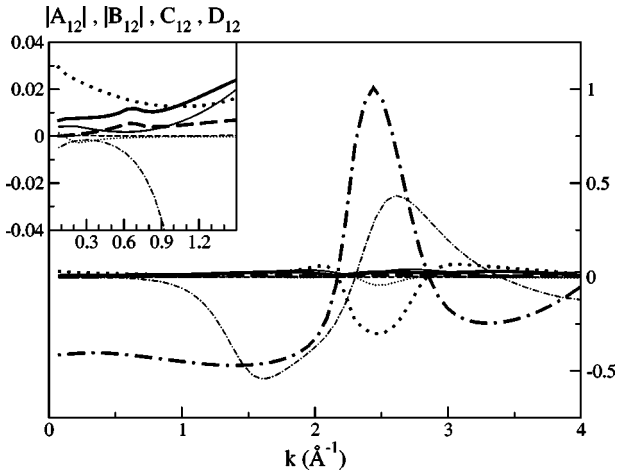


FIG. 11. Amplitudes of the different modes of $F_{12}(k,t)$ for $Li_{0.7}Mg_{0.3}$ (thick lines) and $Li_4Pb$ (thin lines) in the viscoelastic model. Full lines, $A_{12}$; dashed lines, $B_{12}$; dotted lines, $C_{12}$; dash-dotted lines, $D_{12}$.

For medium and large $k$ the dominant term is $z^{(3)}$, the larger real root, with its amplitude $C_{11}$ following $S_{11}(k)$. For small $k$, on the other hand, the situation is different; $D_{11}$ is dominant for $Li_{0.7}Mg_{0.3}$, while for $Li_4Pb$ $C_{11}$ is still the dominant contribution, with an intermediate region around 1.5 $Å^{-1}$, where $D_{11}$ is of similar magnitude. Therefore the overall decay of $F_{11}(k,t)$ is dictated by $z^{(3)}$, which being much larger than $z^{(4)}$ induces a much faster decay; note the smaller scale in the time axis for $F_{11}(k,t)$ in Fig. 8.

It is also interesting to observe that out of the two propagating roots, the dominant one for very small $k$ is the low frequency one, and therefore in this limit all three partials oscillate with the same frequency, as happens within the hydrodynamic model. There is, however, a transition from this behavior to the dominance of the high frequency mode for $k$ values around 0.2 $Å^{-1}$ for $Li_4Pb$ and around 0.5 $Å^{-1}$ for $Li_{0.7}Mg_{0.3}$. This will have a direct impact on the presence of

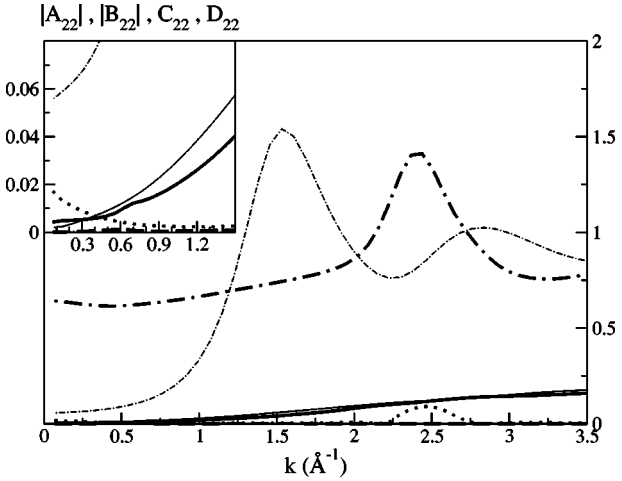


FIG. 12. Amplitudes of the different modes of $F_{22}(k,t)$ for $Li_{0.7}Mg_{0.3}$ (thick lines) and $Li_4Pb$ (thin lines) in the viscoelastic model. Full lines, $A_{22}$; dashed lines, $B_{22}$; dotted lines, $C_{22}$; dash-dotted lines, $D_{22}$.

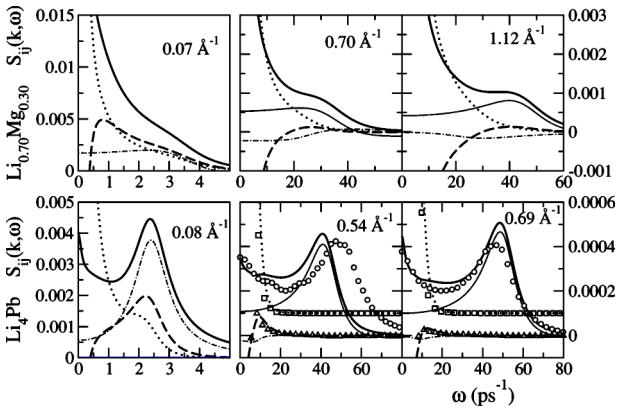


FIG. 13. Dynamic structure factors in units of picoseconds for $Li_{0.7}Mg_{0.3}$ (upper panel) and $Li_4Pb$ (lower panel) at wave vectors shown in the graphs. Full lines, $S_{11}(k,\omega)$; dashed lines, $S_{12}(k,\omega)$; dotted lines, $S_{22}(k,\omega)$. The thin dash-dotted line denotes the low frequency contribution to $S_{11}(k,\omega)$ and the thin full line is the corresponding high frequency contribution, which is negligible for the lowest $k$. Symbols denote simulation data at wave vectors 0.53 and 0.65 $Å^{-1}$ for $Li_4Pb$. For these graphs $S_{22}(k,\omega)$ have been shifted upward by 0.0001 to improve visibility.

low and/or high frequency peaks in the partial DSFs.

In Fig. 13 we show the DSFs for both alloys at a small wave vector, a wave vector in the transition region, and at a larger $k$. In the case of $Li_4Pb$ we observe at the smallest $k$ a clear peak in $S_{11}(k,\omega)$ and $S_{12}(k,\omega)$ and a shoulder in the $S_{22}(k,\omega)$, all at the same frequency, akin to hydrodynamic sound propagation, even though the presence of the diffusive term masks the propagating mode and $S_{22}(k,\omega)$ shows no side peak. For larger $k$ we find a prominent peak in $S_{11}(k,\omega)$ due to the high frequency contribution, while there is no indication of any peak in $S_{22}(k,\omega)$. This appearance of high frequency peaks in the DSF of the light component (11) and its absence in the DSF of the heavy component (22) has been associated with the so called "fast sound" phenomenon, which as we see appears naturally within the viscoelastic model as a consequence of the two propagating roots of the model. In the case of $Li_{0.7}Mg_{0.3}$ the diffusive contribution to $S_{ij}(k,\omega)$ is very large for small $k$, and completely covers the (low frequency) propagating contribution, so that no side peaks appear in the DSFs even for rather small $k$ values. Anyhow this contribution is indeed present and shows up as a rather weak shoulder at the same frequency in all three $S_{ij}(k,\omega)$. For larger $k$ the higher frequency component becomes more important in $S_{11}(k,\omega)$ and due to its larger frequency is less covered by the diffusive contribution, so that for sufficiently large $k$ a peak finally develops in $S_{11}(k,\omega)$, whereas $S_{22}(k,\omega)$, whose dominant propagating contribution is the low frequency one, never develops a side peak. Therefore the situation is rather similar to the case of $Li_4Pb$, except that the separation between the frequencies of the low and the high frequency modes is smaller due to the smaller mass of Mg, and that the magnitude of the diffusive mode in $Li_{0.7}Mg_{0.3}$ definitely obscures the analysis.

Coming to the BT functions, one can expect that $Li_{0.7}Mg_{0.3}$, being a quasi-ideal system, should behave simi-

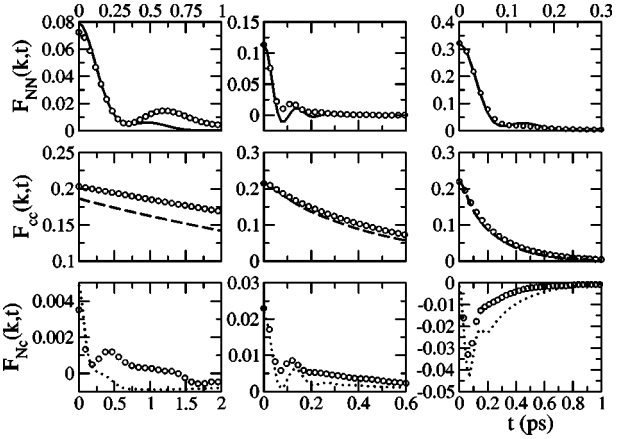


FIG. 14. Bhatia-Thornton ISFs for $Li_{0.7}Mg_{0.3}$. The $k$ values for the different columns are the same as in Fig. 7. Note in some cases the different scales in the time axis for $F_{NN}(k,t)$. Lines are theoretical results and symbols are simulation data.

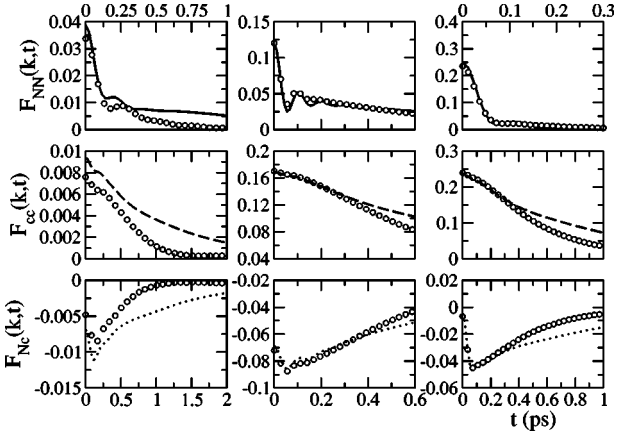


FIG. 16. Bhatia-Thornton ISFs for $Li_4Pb$. The $k$ values for the different columns are the same as in Fig. 8. Lines are theoretical results and symbols are simulation data. Note in some cases the different scales in the time axis for $F_{NN}(k,t)$.

larly to the pseudobinary system, i.e., the single particle dynamics should dominate the concentration-concentration partials, while the collective dynamics should dominate the number-number partials. This is indeed what happens, as shown in Fig. 14, where we see that $F_{NN}(k,t)$ in fact decays much faster than the partials, which is similar to the behavior obtained for the pseudobinary system, $F_{cc}(k,t)$ is practically purely diffusive, as happens for the SISF of a one-component system, and $F_{Nc}(k,t)$ is very much smaller than the two other partials. Obviously this is also reflected in the dynamic structure factors, which are plotted in Fig. 15. $S_{NN}(k,\omega)$ shows clear shoulders or peaks, while $S_{cc}(k,\omega)$ shows neither side peaks nor shoulders (note that for the smallest $k$ shown the MD $F_{Nc}(k,t)$ is too noisy to allow a reliable Fourier transform). On the contrary, the case of $Li_4Pb$ is different, as shown in Figs. 16 and 17. $F_{NN}(k,t)$ now exhibits a certain diffusive component and $F_{cc}(k,\omega)$ does show oscillations. As a consequence, $S_{cc}(k,\omega)$ presents well-defined side peaks or shoulders, indicative of propagating concentration modes. It is important to note that the magnitude of these peaks is very small, around $10^{-5}$, compared to the value of $S_{cc}(k,\omega=0)$, which is far outside the range of the graph, being around $10^{-3}$–$10^{-2}$ depending on the wave vector. We stress that the reproduction of the different behaviors exhibited by the two alloys, even at the level of such small details, represents a stringent test which is well satisfied by the viscoelastic model.

Finally we address the longitudinal current correlation functions. In Fig. 18 we show the AL and the BT functions for $Li_{0.7}Mg_{0.3}$, and in Fig. 19 those corresponding to $Li_4Pb$. Again the case of $Li_{0.7}Mg_{0.3}$ is very similar to pseudobinary Li. For small $k$, the three AL partials have a peak at a common frequency. On the other hand, $C_{12}(k,\omega)$ exhibits both a maximum and a minimum for all $k$, whose positions coincide with the maxima (or shoulders at small $k$) of $C_{11}(k,\omega)$ and $C_{22}(k,\omega)$, respectively. The behavior of the BT currents is also similar to pseudobinary Li: $C_{NN}(k,\omega)$ shows only one peak, and $C_{cc}(k,\omega)$ also shows only one peak, although since the decoupling number-concentration is not complete, a clear

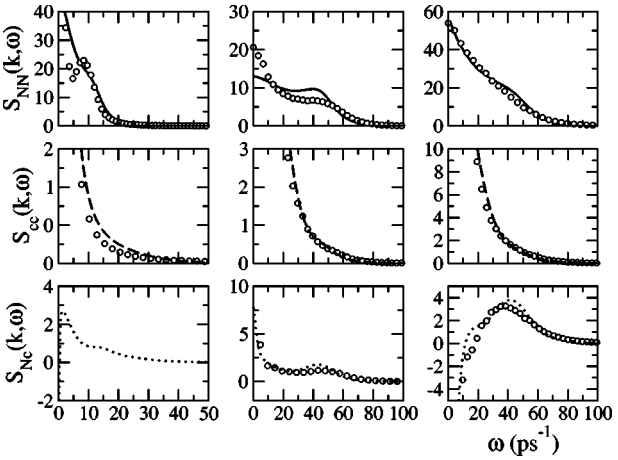


FIG. 15. Bhatia-Thornton DSFs for $Li_{0.7}Mg_{0.3}$ in units of $10^{-4}$ ps. The $k$ values for the different columns are the same as in Fig. 7. Lines are theoretical results and symbols are simulation data.

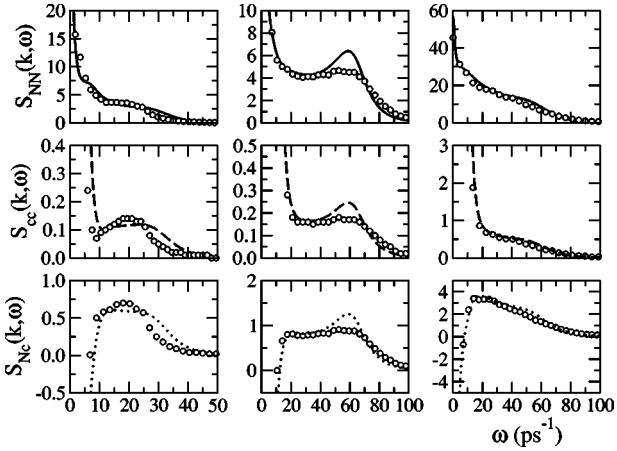


FIG. 17. Bhatia-Thornton DSFs for $Li_4Pb$ in units of $10^{-4}$ ps. The $k$ values for the different columns are the same as in Fig. 8. Lines are theoretical results and symbols are simulation data.

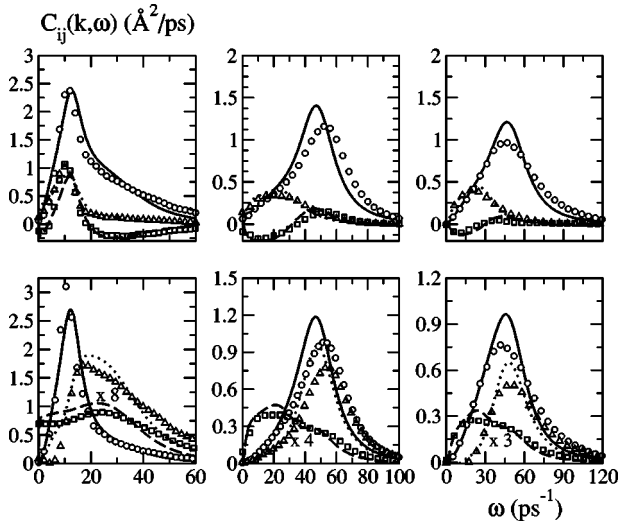


FIG. 18. Longitudinal current correlation functions for $Li_{0.7}Mg_{0.3}$. Lines are theoretical results and symbols are simulation data. Upper panel: Ashcroft-Langreth partials, full line and circles, $C_{11}(k,\omega)$; dashed line and squares, $C_{12}(k,\omega)$; dotted line and triangles, $C_{22}(k,\omega)$ Lower panel: Bhatia-Thornton partials; full line and circles, $C_{NN}(k,\omega)$; dashed line and squares, scaled $C_{cc}(k,\omega)$; dotted line and triangles, scaled $C_{Nc}(k,\omega)$. The $k$ values for the different columns are the same as in Fig. 7.

feature (a shoulder) does also appear at the frequency of the maximum of $C_{NN}(k,\omega)$. In the case of $Li_4Pb$ it is evident that the smallest $k$ shown in the graph is already outside the hydrodynamic region. For all the $k$ values shown we observe two characteristic frequencies, a small one for which we have a maximum in $C_{22}(k,\omega)$ and a maximum (at low $k$) or a minimum (at larger $k$) for $C_{12}(k,\omega)$, and a high one at which there is a maximum in $C_{11}(k,\omega)$ and a minimum (at small $k$) or a maximum (at larger $k$) in $C_{12}(k,\omega)$. The BT currents, on the other hand, always show a common maximum at the high characteristic frequency and a maximum in $C_{cc}(k,\omega)$, minimum in $C_{Nc}(k,\omega)$, at the low one. We therefore see that in $Li_4Pb$ $C_{cc}(k,\omega)$ has a clear double peak structure, each situated close to the low and high frequency roots of the model.

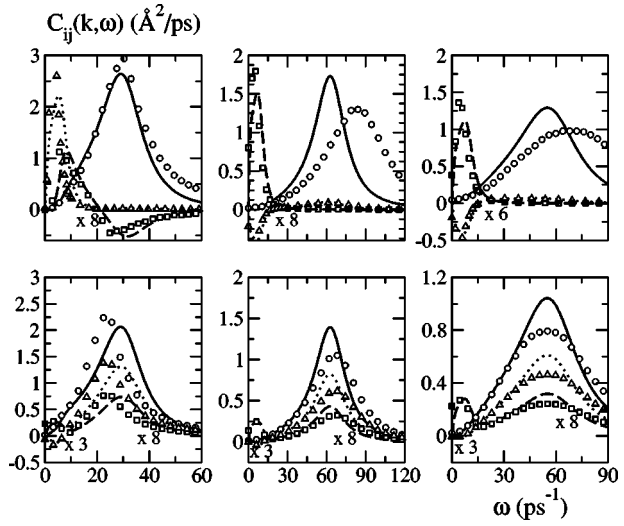


FIG. 19. Longitudinal current correlation functions for $Li_4Pb$. Lines are theoretical results and symbols are simulation data. Upper panel: Ashcroft-Langreth partials. Lower panel: Bhatia-Thornton partials. The meaning of the lines and symbols is the same as in the previous figure. The $k$ values for the different columns are the same as in Fig. 8.

## IV. CONCLUSIONS

We have presented an extension of Lovesey's viscoelastic model to binary mixtures that correctly recovers the same model for the one-component system in the case of pseudobinary mixtures, including both the collective and the single particle properties.

We have observed in the MD simulations of this kind of system a clear appearance of propagating modes in the single particle dynamic properties of the one-component system, specifically in the longitudinal self-current correlation function, which the viscoelastic model reproduces correctly.

In the case of alloys, the appearance of two propagating roots in the model leads naturally to the fast sound phenomenon, which is explained as the dominance of the high frequency propagating contribution in the DSF of the light component, appearing near the $k$ values where the amplitudes of the two propagating roots coincide. For smaller $k$ the amplitude of the high frequency component goes to zero and therefore all the DSFs have a component with a peak at a common frequency, namely, that of the smaller propagating root. Whether this component shows up as a peak or not in the DSFs depends strongly on the amplitude (and width) of the diffusive contributions, which in some cases (like $Li_{0.7}Mg_{0.3}$) can cover the propagating contribution.

The viscoelastic model is able to reproduce the different behaviors of the ISFs of pseudobinary Li and $Li_{0.7}Mg_{0.3}$ on one hand and $Li_4Pb$ on the other. The extremely slow decay of the ISFs for the former two cases is dictated by the small value and large amplitude associated with the smallest real root of the model, which moreover in the case of pseudobinary Li is strictly the single particle contribution. In the case of $Li_4Pb$ a combination of factors leads to a more rapid decay: first, the smallest real root is larger than in $Li_{0.7}Mg_{0.3}$; second, the amplitudes associated with this root in the 22 and 12 partials are much smaller than those in $Li_{0.7}Mg_{0.3}$, due to the behavior of the amplitudes which follow the corresponding partial structure factors; and third, in the case of the 11 partial it is the larger real root that is the dominant one for small $k$, leading therefore to a much faster overall decay. Another important difference is the presence in $Li_4Pb$ of propagating concentration modes, which are absent in $Li_{0.7}Mg_{0.3}$. The presence (or absence) of clear side peaks in $S_{cc}(k,\omega)$ is neatly reproduced by the viscoelastic model, in spite of their very small magnitudes.

We conclude by stressing that although quantitative differences do appear between the results of the model and the simulations as a result of the approximations involved in the former, nevertheless the model reproduces accurately the main characteristic features of the dynamic properties of the systems studied, including very fine details in the peaks of

$S_{cc}(k,\omega)$ and even unexpected peaks in the single particle properties. We believe that this shows that the model is useful and therefore warrants its application to the analysis of data (possibly obtained by any other means) on the dynamic properties of alloys, and on the single particle properties of one-component systems, which will complement the already wide application of the model for the collective dynamics of one-component systems.


## ACKNOWLEDGMENTS

We acknowledge finnancial support from DGICYT (Grants No. MAT2002-04393-C0201 and No. BFM2003-08211-C0302), Junta de Castilla y Leon (Grant No. VA073-02), the NSF (Career Award No. 0133504), and the Army Research Office.


## APPENDIX

Here, we derive the expressions for the matrices $\boldsymbol{\Xi}$ and $\mathbf{K}(\vec{k})$ in the case of a two-component system. In Sec. II B, these matrices were determined by the integral

$$\int_0^\infty dt\, \exp\left(-\frac{t^2}{2}\mathbf{N}(\vec{k},t=0)\right).$$

The exponential is easily performed after diagonalizing $\mathbf{N}(\vec{k},t=0)$. Denoting by $\{\lambda_1(\vec{k}),\lambda_2(\vec{k})\}$ and $\{\mathbf{x}_1(\vec{k}),\mathbf{x}_2(\vec{k})\}$ its eigenvalues and eigenvectors we can write

$$\mathbf{N}(\vec{k},t=0)=\mathbf{P}(\vec{k})\mathbf{N}_D(\vec{k})\mathbf{P}(\vec{k})^{-1} \tag{A1}$$

where $\mathbf{N}_D(\vec{k})$ is a diagonal matrix having the eigenvalues $\{\lambda_1(k),\lambda_2(k)\}$ on the diagonal, whereas $\mathbf{P}(\vec{k})$ is a matrix having $\{\mathbf{x}_1(k),\mathbf{x}_2(k)\}$ as its column vectors. The exponential is then straightforward and the wanted integral is readily evaluated leading to

$$\tilde{\mathbf{M}}(\vec{k},z=0)=\frac{\sqrt{\pi}}{2}\boldsymbol{\Xi}\ \mathbf{P}(\vec{k})\mathbf{D}(\vec{k})\mathbf{P}(\vec{k})^{-1}\ \mathbf{M}(\vec{k},t=0) \tag{A2}$$

where $\mathbf{D}(\vec{k})$ is a diagonal matrix with elements $\{\sqrt{2/\lambda_1(k)},\ \sqrt{2/\lambda_2(k)}\}$ on the diagonal. Now, by using Eq. (18), it is obtained that

$$\tilde{\mathbf{F}}(\vec{k},z=0)=\frac{2}{\sqrt{\pi}}[\boldsymbol{\Xi}\mathbf{P}(\vec{k})\mathbf{D}(\vec{k})\mathbf{P}(\vec{k})^{-1}\mathbf{M}(\vec{k},t=0)]^{-1}\mathbf{F}(\vec{k},t=0) \tag{A3}$$

and by examining the $k\to\infty$ limit of this equation, the elements of the matrix $\boldsymbol{\Xi}$ are obtained. In particular we have

$$\lambda_i(\vec{k}\to\infty)=\frac{2k^2k_BT}{m_i},$$

$$\mathbf{P}(\vec{k}\to\infty)=\mathbf{I},$$

$$[\mathbf{M}(\vec{k}\to\infty,t=0)]_{ij}=\delta_{ij}\frac{k^2k_BT}{m_i},$$

$$[\tilde{\mathbf{F}}(\vec{k}\to\infty,z=0)]_{ij}=\pi S_{ij}(\vec{k},\omega=0)=\delta_{ij}\left(\frac{\pi}{2k^2}\frac{m_i}{k_BT}\right)^{1/2} \tag{A4}$$

leading to $\boldsymbol{\Xi}=(2\sqrt{2}/\pi)\mathbf{I}$.

Now, we turn to the determination of the matrix $\mathbf{K}(\vec{k})$. By inserting Eq. (A2) in Eq. (25), and using the previous result for $\boldsymbol{\Xi}$, it is obtained that

$$\mathbf{K}(\vec{k})=\frac{\sqrt{\pi}}{2}\mathbf{P}(\vec{k})\mathbf{D}(\vec{k})\mathbf{P}(\vec{k})^{-1}. \tag{A5}$$

The explicit expressions for the matrix elements of $\mathbf{K}(\vec{k})$ are

$$K_{11}(\vec{k})=\frac{2}{\sqrt{\pi}}\frac{N_{12}(\vec{k})N_{21}(\vec{k})\lambda_1^{1/2}(\vec{k})+\beta^2(\vec{k})\lambda_2^{1/2}(\vec{k})}{N_{12}(\vec{k})N_{21}(\vec{k})+\beta^2(\vec{k})},$$

$$K_{12}(\vec{k})=\frac{2}{\sqrt{\pi}}\frac{N_{12}(\vec{k})\beta(\vec{k})[\lambda_1^{1/2}(\vec{k})-\lambda_2^{1/2}(\vec{k})]}{N_{12}(\vec{k})N_{21}(\vec{k})+\beta^2(\vec{k})},$$

$$K_{21}(\vec{k})=\frac{2}{\sqrt{\pi}}\frac{N_{21}(\vec{k})\beta(\vec{k})[\lambda_1^{1/2}(\vec{k})-\lambda_2^{1/2}(\vec{k})]}{N_{12}(\vec{k})N_{21}(\vec{k})+\beta^2(\vec{k})},$$

$$K_{22}(\vec{k})=\frac{2}{\sqrt{\pi}}\frac{N_{12}(\vec{k})N_{21}(\vec{k})\lambda_2^{1/2}(\vec{k})+\beta^2(\vec{k})\lambda_1^{1/2}(\vec{k})}{N_{12}(\vec{k})N_{21}(\vec{k})+\beta^2(\vec{k})}, \tag{A6}$$

where the $N_{ij}(\vec{k})$ are the matrix elements of $\mathbf{N}(\vec{k},t=0)$, the eigenvalues are given by

$$\lambda_1(\vec{k})=\frac{1}{2}\left[N_{11}(\vec{k})+N_{22}(\vec{k})\right]+\left[\left(\frac{N_{11}(\vec{k})-N_{22}(\vec{k})}{2}\right)+N_{12}(\vec{k})N_{21}(\vec{k})\right]^{1/2},$$

$$\lambda_2(\vec{k})=\frac{1}{2}[N_{11}(\vec{k})+N_{22}(\vec{k})]-\left[\left(\frac{N_{11}(\vec{k})-N_{22}(\vec{k})}{2}\right)+N_{12}(\vec{k})N_{21}(\vec{k})\right]^{1/2}, \tag{A7}$$

and $\beta(\vec{k})=\lambda_1(\vec{k})-N_{11}(\vec{k})$.

[1] Ya. Chusak, T. Bryk, A. Baumketner, G. Kahl, and J. Hafner, Phys. Chem. Liq. **32**, 87 (1996).
[2] N. Anento, J. Casas, M. Canales, D. J. González, L. E. González, and J. A. Padró, J. Non-Cryst. Solids **250–252**, 348 (1999).
[3] S. W. Lovesey, J. Phys. C **6**, 1856 (1973).
[4] J. R. D. Copley and S. W. Lovesey, Rep. Prog. Phys. **38**, 461 (1975).
[5] W. E. Alley and B. Alder, Phys. Rev. A **27**, 3158 (1983); B. Kamgar-Parsi, E. G. D. Cohen, and I. M. de Schepper, *ibid.* **35**, 4781 (1987).
[6] D. L. Price and J. R. D. Copley, Phys. Rev. A **11**, 2124 (1975).
[7] I. M. de Schepper, E. G. D. Cohen, C. Bruin, J. C. van Rijs, W. Montfrooij, and L. A. de Graaf, Phys. Rev. A **38**, 271 (1988).
[8] T. Bryk, I. Mryglod, and G. Kahl, Phys. Rev. E **56**, 2903 (1997).
[9] N. W. Ashcroft, Phys. Lett. **23**, 48 (1966).
[10] N. Anento, J. A. Padró, O. Alcaraz, and J. Trullàs, Mol. Simul. **29**, 373 (2003).
[11] M. Canales, D. J. González, L. E. González, and J. A. Padró, Phys. Rev. E **58**, 4747 (1998).
[12] A. P. Copestake, R. Evans, H. Ruppersberg, and W. Schirmacher, J. Phys. F: Met. Phys. **13**, 1993 (1983).
[13] N. Anento and J. A. Padró, Phys. Rev. B **62**, 11428 (2000).
[14] N. Anento and J. A. Padró, J. Chem. Phys. **116**, 6159 (2002).
[15] J. Bosse, G. Jacucci, M. Ronchetti, and W. Schirmacher, Phys. Rev. Lett. **57**, 3277 (1986).
[16] R. Fernández-Perea, M. Alvarez, F. J. Bermejo, P. Verkerk, B. Roessli, and E. Enciso, Phys. Rev. E **58**, 4568 (1998).
[17] L. E. González, D. J. González, and M. Silbert, Phys. Rev. A **45**, 3803 (1992).
[18] M. Canales, L. E. González, and J. A. Padró, Phys. Rev. E **50**, 3656 (1994).
[19] T. Bryk and I. Mryglod, Phys. Rev. E **63**, 051202 (2001).
[20] A. Baumketner, Ph.D. thesis, Institute for Condensed Matter Physics, National Academy of Sciences of Ukraine Lviv, 2000.
[21] N. W. Ashcroft and N. D. Mermin, *Solid State Physics* (Holt-Saunders, Philadelphia, 1976).
[22] N. Anento and J. A. Padró, Phys. Rev. E **64**, 021202 (2001).